Local Dynamics of Syndiotactic Poly(methyl methacrylate) Using Molecular Dynamics Simulation

Chunxia Chen[†] **and Janna K. Maranas***

Department of Chemical Engineering, The Pennsylvania State University, University Park, Pennsylvania 16802

Victoria García-Sakai[‡]

NIST Center for Neutron Research, National Institute of Standards and Technology, Gaithersburg, Maryland 20899-8562

ABSTRACT: The local dynamics of syndiotactic poly(methyl methacrylate) (PMMA) are investigated by explicit atom molecular dynamics (MD) simulations and quasielastic neutron scattering at temperatures well above the glass transition temperature. Using MD, we are able to isolate specific local motions well above T_g. These include rotations of the α-methyl and ester methyl, rotations of the entire ester side group and segmental motion of the chain backbone. This capacity is unique to simulation as proton motion at high temperatures necessarily involves multiple motions. The force field used is validated by direct comparison to structural and dynamic neutron scattering measurements, and by comparison via temperature extrapolation of activation energies and rotational times for methyl group rotations. We find that the rotation of the ester side group is consistent with the β-relaxation at low temperatures: the activation energy closely matches that assigned from dielectric spectroscopy (DS), and relaxation times are also consistent with these measurements. Although the ester protons rotate continuously with no preferred spatial orientation, the rotation of the ester oxygen around the C_1−C bond [O−C−C_1−C_3] does appear to be a 2-fold jump as observed in NMR experiments. The α-relaxation is associated with the motion of the main chain. Relaxation times for these protons are not Arrhenius, but rather begin to diverge as the temperature is lowered. Rotation of the slower α-CH_3 group occurs with rates similar to the α- and β-relaxations in the temperature range we investigate. Both this rotation and that of the ester side group are more prominent at smaller scales and explain why neutron scattering measurements on PMMA reveal the α-relaxation as the spatial scale is increased.

I. Introduction

The dynamic processes of glass forming systems have been widely investigated using a variety of techniques including NMR,[1] dielectric spectroscopy (DS),[2−4] and light[5] and neutron[4,6] scattering. The α-relaxation, which arrests at the glass transition temperature T_g, is commonly associated with the segmental relaxation of the main chain. Polymer molecules, especially those with side groups, have other relaxation processes known as secondary relaxations.[7−9] Poly(methyl methacrylate) [PMMA] is one such polymer and its repeat unit is illustrated in Figure 1. Secondary processes in PMMA include rotations of the ester and α-methyl groups and the β-relaxation, which has been linked with the reorientation of the entire ester side group around the C−C bond linking it to the backbone. At temperatures well above T_g all processes are active; below T_g the segmental relaxation is frozen and only secondary relaxations are active. As a result, at temperatures above T_g, secondary motions may merge with those of the main chain making individual assessment difficult.

The β-relaxation is normally prominent in dielectric measurements for PMMA. 2D and selective-excitation 3D exchange NMR techniques[10] have been applied to explore the molecular motion underlying the β-relaxation in PMMA below T_g. These experiments show that the OCO plane of the side group undergoes 180° flips which are related to the β-relaxation. This side-group flip is accompanied by a main chain rearrangement.
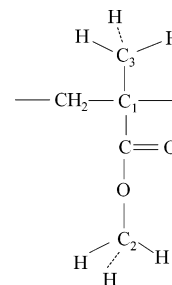
* Corresponding author. E-mail: jmaranas@psu.edu.
† E-mail: cqc10@psu.edu.
‡ Email address: vicky@nist.gov.

Figure 1. Chemical structure of the repeat unit of PMMA.

Recently our group initiated a quasi-elastic neutron scattering [QENS] study of the segmental dynamics of PMMA and how they are influenced by blending with poly(ethylene oxide) [PEO].[11] This neutron measurement showed that pure PMMA displays different relaxation behavior at different spatial scales. At spatial scales larger than the interchain peak, relaxation times increase rapidly as the temperature is decreased toward the glass transition temperature: typical for the α-relaxation. At intrachain spatial scales the temperature dependence of relaxation times is Arrhenius with an activation energy of 118 kJ/mol, consistent with the merged αβ process. These experiments were performed above T_g and thus potentially include contributions from all motions, including secondary relaxations in PMMA.

Rotation of the methyl groups is the most straightforward motion in PMMA. This rotation is often approximated by an effective one-dimensional single particle potential, and is usually represented by instantaneous jumps between three equidistant sites on a circle.[12,13] The resulting rotational motion often falls

CDV

Table 1. EA Model Parameters

$$u^{nb}(r_{ij}) = 4\epsilon[(\sigma/r)^{12} - (\sigma/r)^6] + (1/4\pi\epsilon_0)(q_i q_j/r_{ij})$$

nonbonded interaction	atom	σ (Å)	ϵ (kcal/mol)	q_i (e.c.)
C3	C in CH$_3$ group connected to main chain	3.52	0.067	−0.135
C2	C in CH$_2$ group	3.52	0.067	−0.09
C	C in the main chain	3.20	0.051	0.00
CD	C connect to O by double bond	3.75	0.105	0.51
OD	O connected to C by double bond	2.96	0.210	−0.43
O	O in ester group	3.00	0.170	−0.33
CO	C in CH$_3$ group connected to ester O	3.50	0.066	0.16
H	H in alkane CH$_3$ or CH$_2$ groups	2.50	0.030	0.045
HO	H in ester OCH$_3$ group	2.42	0.015	0.030

	$u^{bond}(r_{ij}) = k_{bond}(r_{ij} - r_{ij}^0)^2$			$u^{bond}(r_{ij}) = k_{bond}(r_{ij} - r_{ij}^0)^2$	
bonds	k_{bond} (kcal/mol/Å^2)	r_{ij}^0 (Å)	bonds	k_{bond} (kcal/mol/Å^2)	r_{ij}^0 (Å)
C3−C	368	1.539	CD−O	471	1.360
C2−C	300	1.5491	CO−O	342	1.446
CD−C	326	1.517	CT−HT[a]	331	1.09
CD−OD	968	1.209	CO−HO	331	1.09

	$u^{bend}(\theta_{ijk}) = k_{bend}(\theta_{ijk} - \theta_{ijk}^0)^2$			$u^{bend}(\theta_{ijk}) = k_{bend}(\theta_{ijk} - \theta_{ijk}^0)^2$	
bends	k_{bend} (kcal/mol/rad^2)	θ_{ijk}^0 (deg)	bends	k_{bend} (kcal/mol/rad^2)	θ_{ijk}^0 (deg)
C−C2−C	89.5	113.3	CD−O−CO	84.8	116.4
CT−C−CT	87.9	109.47	H−CT−C	35.0	109.5
CT−C−CD	87.9	109.47	H−CT−H	35.0	109.5
C−CD−O	74.5	111.4	HO−CO−HO	35.0	109.5
C−CD−OD	63.3	125.6	HO−CO−O	56.0	110.1
OD−CD−O	126.5	123.0			

	$u^{inversion}(\theta_{ijk}) = K_1(\theta_{ijk} - \theta_0) + K_2(\theta_{ijk} - \theta_0)^2$		
inversion	θ_0 (deg)	K_1 (kcal/mol/rad)	K_2 (kcal/mol/rad^2)
CD	360	−60.0	30.0

	$u^{torsion}(\phi_{ijkl}) = V_1(1 + \cos(\phi_{ijkl})) + V_2(1 - \cos(2\phi_{ijkl})) + V_3(1 + \cos(3\phi_{ijkl})) + V_4(1 - \cos(4\phi_{ijkl}))$			
torsions (kcal/mol)	V_1	V_2	V_3	V_4
CT−C−C2−C	0.277 92	0.000 00	0.000 00	−0.277 92
CD−C−C2−C	0.277 92	0.000 00	0.000 00	−0.277 92
CT−C−CD−O	0.807 84	0.000 00	0.000 00	−0.807 84
CT−C−CD−OD	2.600 00	0.050 00	−2.550 00	0.000 00
C−O−C−C	2.020 00	−1.000 00	−0.700 00	−0.320 00

[a] CT includes C3 and C2; HT includes H and HO

within the experimental frequency range of neutron scattering at temperatures below T_g. This technique, combined with deuterium labeling, has been successfully employed to investigate the rotational dynamics of ester methyl group rotations.[14−17] Rotation of the α-methyl is slower and not as thoroughly investigated.[18]

As discussed above, at higher temperatures the relaxation of PMMA appearing in the QENS window is a combination of α-methyl group rotation, ester methyl group rotation, β-relaxation, and α-relaxation. It is therefore difficult to retrieve specific local motions using this technique even with deuterium labeling, because the same protons may participate in more than one type of motion. In the current contribution, we use molecular dynamics simulation to separate these motions. Simulations also allow us to explore and validate specific mechanisms for motion directly: for example, the association of the α-relaxation with motion of the chain backbone, and connection of the β-relaxation to the rotation of the ester side group. At the same time, only a few works have been done on PMMA MD simulations[19−21] and therefore we also propose a force field for this purpose and validate it against QENS data.

The outline of the paper is as follows. In section II, we give the details of the computational model, and in section III, the details of the experiments (neutron diffraction and quasielastic neutron scattering) are discussed. Force field validation by comparison of PMMA structure and dynamics to neutron experiments is given in section IV, while in section V the local dynamics including methyl group rotation, the entire ester side group rotation, and the main chain motion are discussed. Finally in section VI, a summary and conclusion are given.

II. Simulation Details

Model. We perform explicit atom (EA) simulations on a system of 27 PMMA chains of 200 atoms with 100% syndiotactic sequences, and thus the simulated PMMA has a molecular weight of 1316 g/mol. We run the simulations under conditions of constant volume and temperature (*NVT* ensemble). A series of temperatures are considered: 400, 420, 450, 470, 500, 520, 550, and 600 K. The temperatures are held constant using the velocity-rescaling algorithm of Berendsen et al.[22] The simulation box size is chosen to match the PMMA density.[23] The system was initially simulated at 500 K. Higher and lower temperatures were reached by cooling or heating in stages, allowing for equilibration at each stage. These temperatures are all above the glass transition temperature of PMMA (373 K), as determined by DSC measurements on a low molecular weight PMMA sample (see experimental details).

We use the OPLS force field[24,25] as detailed in Table 1. The cutoff distance for the nonbonded interactions is 8 Å, and the Ewald summation[26,27] method was used to calculate long-range

CDV

Table 2. Corresponding Time Step for Different Interactions

interaction type	time step, fs
bonding, bending and torsion	1
van der Waals and the real part of the Coulomb Ewald summation	2
reciprocal part of the Coulomb Ewald summation	4

Coulomb interactions. To increase computational efficiency we used the multiple time step reversible reference system propagator algorithm [rRESPA],[28,29] with timesteps as detailed in Table 2.

To generate initial configurations for our EA simulations, we begin with equilibrated united atom (UA) coordinates from prior runs. Hydrogen atoms are inserted on the equilibrated carbon positions as follows. The hydrogen atoms on the main chain [CH$_2$ group] are inserted by fixing C−C−H bond angles at 110° and the C−H bond lengths at 1.09 Å. For the CH$_3$ groups, we first insert one hydrogen atom by fixing C−C−H (for α-methyl group) or O−C−H (for ester methyl group) bond angles at 110° and the C−H bond length at 1.09 Å. The remaining two hydrogen atoms were then reinserted by fixing H−C−H bond angles at 110° and C−H bond lengths at 1.09 Å.

Equilibration. The EA configuration prepared as described above is further equilibrated for at least 4 ns before collecting data, followed by production runs of 6 ns. This equilibration time is selected such that the atoms have moved a distance comparable to their chain dimensions. No shifts in structural or dynamic properties are evident as illustrated by the self-intermediate scattering function $S(q,t)$ in Figure 2, calculated over three 2 ns blocks following the proposed equilibration time of 4 ns. These results suggest that the equilibration time is sufficient.
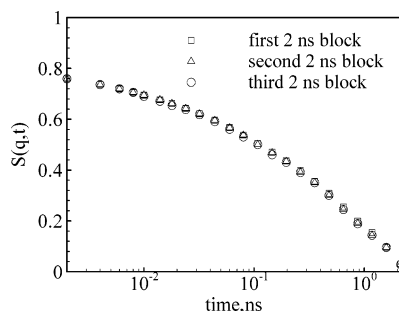

Figure 2. Representative self-intermediate scattering function calculated over 2 ns blocks to illustrate the lack of drift in dynamic properties at $q = 0.8$ Å^{-1} and $T = 500$ K.

III. Experimental Details

To validate the chosen force field, we use both structural and dynamic neutron measurements. The structural measurements were performed on a sample of 80% syndiotactic sequences and a molecular weight of 375 000 g/mol. They are described in ref 30. Two quasielastic neutron scattering measurements to assess dynamics are discussed below. These measurements were performed at the NIST Center for Neutron Research in Gaithersburg, MD.

High-Flux Backscattering Spectrometer[31] [HFBS]. In this spectrometer, neutrons of incident wavelength 6.271 Å ($E_0 = 2.08$ meV) are Doppler shifted to achieve a range of incident energies (±20 μeV) about this nominal value. The neutrons are scattered by the sample, after which only those neutrons with a final energy of 2.08 meV are detected. The dynamic range (energy transfer) of ±20 μeV sets the shortest time available to the instrument. The instrumental resolution (full width at half-maximum), which sets the longest time, is dependent on the size of the Doppler shift and equal to 0.87 μeV for ±20 μeV. For data reduction purposes, this resolution was measured with a vanadium sample at 295 K. The

pressed polymer sample was held in a cylindrical aluminum can mounted on a closed cycle refrigerator unit. The thickness of the sample was around 0.1 mm, chosen to achieve 90% neutron transmission and minimize multiple scattering. The PMMA was purchased from Polymer Standards Service and has a molecular weight of 463 000 g/mol and 76% syndiotactic sequences.

Disk Chopper Time-of-Flight Spectrometer[32] [DCS]. The disk chopper spectrometer uses a fixed incident wavelength, and energies of scattered neutrons are resolved by their flight times. The spectrometer was operated at an incident wavelength of 4.2 Å and at a resolution of 80 μeV. The instrumental resolution was measured using a vanadium sample at 295 K with the same instrument configuration. The measured QENS spectra collected over 6 h periods were corrected for detector efficiencies using software developed at NIST (Data Analysis and Visualization Environment, DAVE).[33] The scattering from the empty aluminum can and from the background were subtracted and the data were binned into q-groups in the range 0.60−2.60 Å^{-1}. As with HFBS, the sample was annular in shape and held in a thin-walled aluminum can mounted onto a closed-cycle refrigerator, and of thickness of 0.1 mm to minimize multiple scattering. Two hydrogenated PMMA samples were used: the one described for HFBS [463 000 g/mol and 76% syndiotactic], and one closer to the simulated molecular weight [3500 g/mol], with the same percentage of syndiotactic sequences. The glass transition temperatures measured by DSC are 397 and 373 K, respectively.

Both HFBS and DCS experiments are performed at 500 K and measure the scattering intensity as a function of energy and momentum transfers, which sets the time and spatial scales, respectively. The momentum transfer is related to spatial scale by $q = 2\pi/r$ and the energy transfer to time by $t = h/\Delta E$. In order to combine the neutron scattering data from DCS and HFBS and compare these data to simulation results, the scattering functions were Fourier transformed to the time domain as discussed in refs 11 and 34.

The contribution of a single scattering event to the total scattering depends on the scattering cross sections of the atoms involved; both incoherent [self-motion] and coherent [relative motion] cross sections must be considered. Incoherent scattering reflects correlations between the same atom at different times, while coherent scattering reflects relative positions of atomic pairs. In the static case (diffraction experiment), the sample must be mostly deuterated and it reveals the corresponding sum of partial static structure factors. As the incoherent cross section of the proton is substantially larger than all others, the QENS experiments are performed on hydrogenated samples for which the incoherent scattering from hydrogen represents 93% of the total. The QENS results reported here thus represent the self-motion of protons. Further, in the comparisons of simulation to QENS experimental experiments, we neglect coherent contributions when computing dynamic observables from simulation coordinates.

IV. Validation of the Simulation Model

To check the performance of the OPLS force field, we compare the static structure factor $S(q)$ and the self-intermediate scattering function $S(q,t)$ obtained from the simulation to available neutron scattering measurements in ref 30 and described above.

We calculate the static structure factor $S(q)$ assuming an isotropic sample using[35]

$$S(q) = \frac{n}{\langle |b|^2 \rangle} \sum_i \sum_j c_i c_j b_i b_j \int_0^\infty [g_{ij}(r) - 1] \frac{\sin qr}{qr} 4\pi r^2 \, dr \tag{1}$$

where

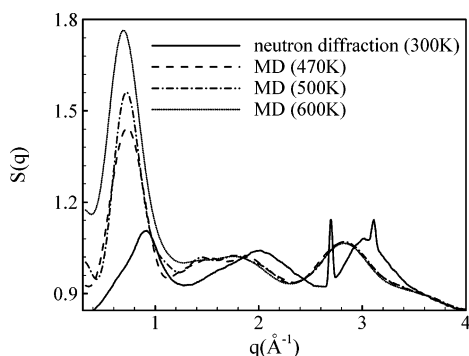$$\langle |b|^2 \rangle = \sum_i c_i |b_i|^2 \tag{2}$$

CDV

Figure 3. Comparison of the static structure factor of syndiotactic PMMA calculated from simulations at temperatures of 470, 500, and 600 K with neutron diffraction experiments.[30]

and

$$g_{ij}(r) = \frac{V}{4\pi r^2 n^2} \left\langle \sum_i \sum_{j \neq i} \delta(r - r_{ij}) \right\rangle \quad (3)$$

In the above, i and j represent different atomic species, the coherent scattering length b describes the interaction between neutron and nucleus, c is the atomic species concentration, and the radial distribution function $g_{ij}(r)$ reflects the local packing between atoms of types i and j. As the static structure factor $S(q)$ is normally measured on deuterated samples, we use the coherent scattering length for deuterium rather than hydrogen.

Figure 3 compares the static structure factor of PMMA calculated from eqs 1−3 at 470, 500, and 600 K to neutron diffraction experiments at room temperature.[30] Note that the experimental data have been renormalized to match with the simulation data at high q. The sharp peaks at $q = 2.7$ Å^{-1} and $q = 3.1$ Å^{-1} in the experimental data are due to the diffraction of the aluminum sample holder. In the investigated q range all data sets show three peaks. The first [lowest q] peak shifts to smaller q values and becomes more intense with increasing temperature, while the second and the third peaks are insensitive to temperature. These results suggest that the first peak represents intermolecular correlations while the second and third peaks reflect intramolecular packing. The height and location of the intermolecular peak obtained from the simulation depends strongly enough on temperature that the disagreement between experiment [300 K] and simulation [lowest temperature 470 K] could be attributed to temperature dependence. Differences in the second and third peaks reflect a different intramolecular distribution (bond and torsional angles), most likely due to the sequence distribution, which is 100% syndiotactic for the simulations and 80% syndiotactic for the experimental sample.

The self-intermediate structure factor $S(q,t)$ describes the mobility of atoms in the system. We obtain this directly from the molecular dynamics trajectory,

$$S(q,t) = \frac{1}{N} \left\langle \left| \sum_{i=1}^{N} \exp[-i\vec{q} \cdot (\vec{r}_i(t + t_0) - \vec{r}_i(t_0))] \right| \right\rangle =$$

$$\frac{1}{N} \left\langle \left| \sum_{i=1}^{N} \cos(q \cdot |x_i(t + t_0) - x_i(t_0)|) \right| \right\rangle \quad (4)$$

where $\bar{r}_i(t)$ is the distance vector of atom i at time t, and $x_i(t)$ the x coordinate of $\bar{r}_i(t)$. To compare with DCS and HFBS experiments in which the signal is dominated by hydrogen atoms, we include only hydrogen atoms in the calculation of $S(q,t)$. Plotted in Figure 4 is the $S(q,t)$ from simulation and DCS and HFBS experiments at two q values (0.9 Å^{-1} and 1.5 Å^{-1})
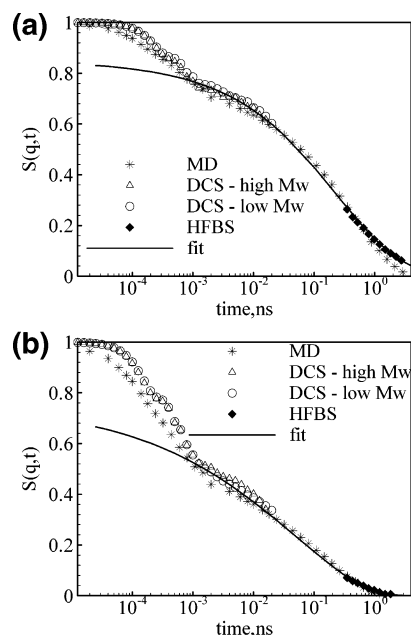

Figure 4. Comparison of the incoherent dynamic structure factors of PMMA from simulations with DCS and HFBS measurements at 500 K at two q values: (a) $q = 0.9$ Å^{-1}; (b) $q = 1.5$ Å^{-1}.

at 500 K. For the experimental data, a fit line is also given to estimate the decay in the time gap between the two instruments. Two things should be noted: the simulations are in reasonable agreement with experiments and different molecular weight samples yield almost identical DCS results. This indicates that molecular weight has little effect on the local dynamics of PMMA, and that the simulation model provides fair description of dynamics of real PMMA samples. The fits indicated in this figure are described below.

V. Local Dynamics

Above we provided evidence that the simulation model we adopted is able to capture both structural and dynamic properties of PMMA. We now use this model to analyze and separate the local dynamics of PMMA at high temperatures: ester and α-methyl group rotations, rotation of the entire ester side group and main chain motion. Before going into the details of these motions, it should be noted that in this paper we always calculate neutron observables: the local dynamics are represented by the self-intermediate scattering function calculated through eq 4 and in our calculations only hydrogen motion is included. To isolate rotation around a specific bond, translational motion of the terminal atom of that bond must be removed. We thus calculate $S(q,t)$ using eq 4 but "virtually fixing" the terminal position of the rotating group. Virtually fixing refers to removing contributions from translational motion by calculating hydrogen positions relative to the position of the appropriate carbon atom. As examples, in ester methyl group rotation the position of C_2 [in Figure 1] is fixed, whereas for rotation of the entire ester side group, the position of C_1 [in Figure 1] is fixed. Clearly, these carbon atoms do move throughout the simulation: their position is rendered fixed by calculating the hydrogen positions relative to the position of the appropriate carbon atom.

A. α-Methyl and Ester Methyl Group Rotation. As discussed in the Introduction, it is challenging to use QENS to investigate ester CH_3 group rotation at high temperatures; even with selective deuteration, the position of atom C_2 will translate such that rotation cannot be isolated. The resulting motion would be fit using a combination of translational and rotational models,
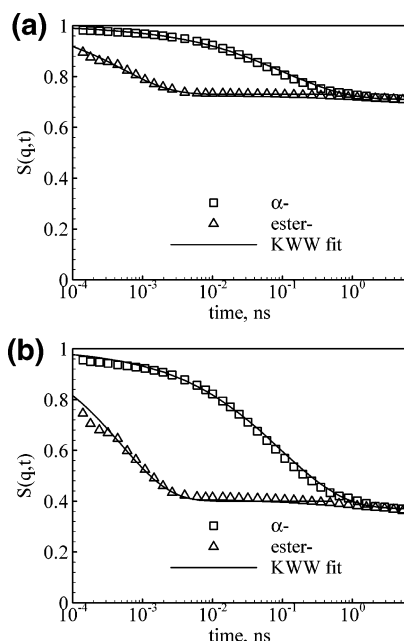
CDV

Figure 5. Rotational $S(q,t)$ for α-methyl and ester CH_3 groups at 500 K and two q values: (a) $q = 0.9$ Å^{-1}; (b) $q = 1.5$ Å^{-1}. The KWW fits are for the long-time decay ($t > 0.3$ ps).

which require assigning a large number of fit parameters from a small decay. Although experimental reports of ester CH_3 rotation are available in the temperature range of 80−200 K,[15] little information is available for α-methyl group rotation. Genix et al.[36] provide some simulation data for α-methyl and ester methyl group rotation, but only at 400 K, which is close to the T_g of PMMA. We separate both rotations from other motions, and thus provide data for both methyl rotations at high temperatures. As explained above we isolate rotation by fixing the terminal position of the rotating group, the dynamics of methyl group rotation are thus calculated from eq 4 by taking the relative distance between hydrogen atoms and the carbon atom positions they are bonded to. Figure 5 shows the rotational $S(q,t)$ for α- and ester CH_3 groups at two q values. It can be seen from the graphs that two processes contribute. The short time (<0.3 ps) process, which is more prominent for the ester methyl, results from internal vibrations within molecules, and is followed by decay due to the rotation of the ester methyl group. At long times, $S(q,t)$ decays to an almost constant value for both methyl group rotations. The plateau in $S(q,t)$ indicates the presence of an elastic incoherent structure factor [EISF]. Physically this indicates motion over a restricted spatial area, and the q dependence of the EISF characterizes the geometry of that spatial area. In the case of CH_3 rotation, a 3-fold rotation[37,38] is often used: the protons jump between three equivalent sites. This results in a temperature-independent EISF of the form:[39]

$$\text{EISF} = \frac{1}{3}\left[1 + 2\frac{\sin{(qr_{H-H})}}{qr_{H-H}}\right] \quad (5)$$

where $r_{H-H} = 1.78$ Å is the H−H distance.

Figure 6 compares the EISF calculated from 3-fold, as well as 4-fold and 6-fold rotation models and that obtained from the plateau value in the simulations. As can be seen from the figure, the EISF obtained from the simulation is temperature independent and consistent with the prediction from all three rotational models at q values lower than 1.8 Å^{-1}. At larger q, the simulated data is more consistent with 4- and 6-fold rotation models.
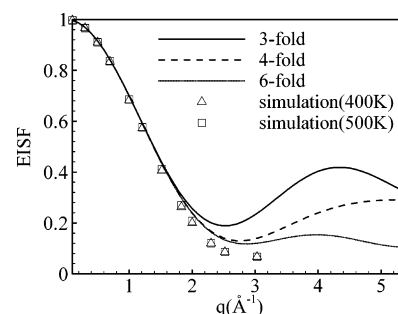

Figure 6. q dependence of the simulated EISF compared to theoretical predictions for CH_3 rotation in 3-fold, 4-fold, and 6-fold models.
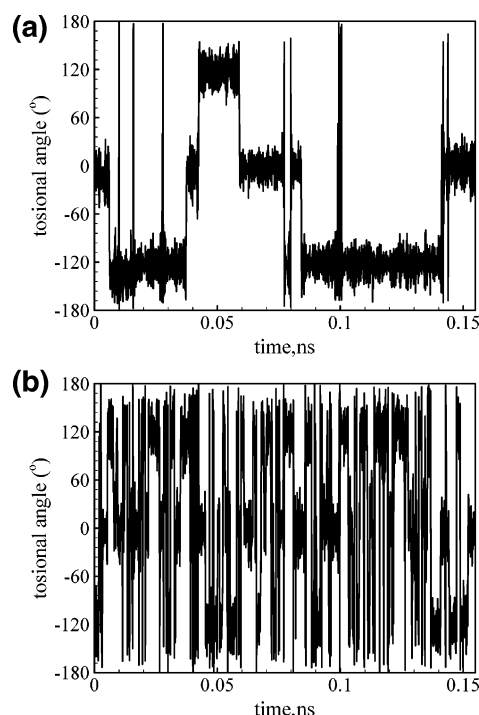

Figure 7. Dihedral angle as a function of time with the time interval of 0.04 ps: (a) α-methyl group; (b) ester methyl group at 500 K.

QENS experimental data on the methyl group rotation of polyisoprene appear to be consistent with 3-fold rotation,[40] but they are only available for q values lower than 2 Å^{-1} due to instrumental limitations. Moreno and colleagues[13,14] found that a 6-fold correction to the 3-fold potential was required to describe rotation of the methyl group in PMMA and in glassy toluene.

In any of the rotational jump models, it is presumed that the rotating atoms jump between the designated number of sites, with the residence time in each site being much larger than the time required to change from site to site. In addition, rotational models neglect librational motion within each site. These requirements will clearly be satisfied at low temperatures. It is possible that at high temperatures, the residence times will become so small that the total amount of time a proton spends in rotational sites is roughly equal to the time it spends jumping from one site to another. This could result in an EISF that does not reflect the true nature of the rotation. To address this issue, we have calculated the torsional angle of a proton in each type of methyl group at 500 K as a function of time. The results are presented in Figure 7, where it is apparent that the torsional angle of the α proton [H−C_3−C_1−C] undergoes librational motion in each of three different sites [−120, 0, and 120°], punctuated by quick jumps between sites, as expected. The
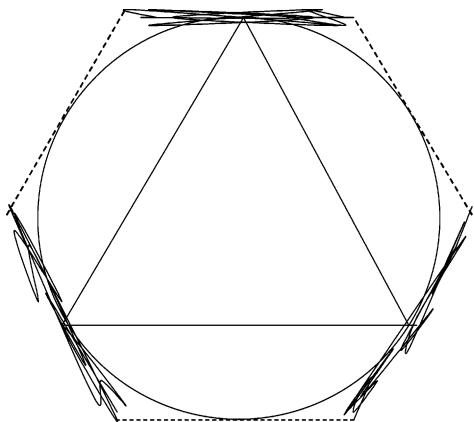
CDV

Figure 8. Schematic of a methyl rotation on a circle. Dashed lines represent proton jumps between different energy levels. Solid lines represent librational motion. The triangle indicates an ideal 3-fold jump and the hexagon represents an approximated 6-fold jump.

torsional angle of the ester proton [H−C_2−O−C] also occupies three sites, but as the jumps between them are far more frequent, the proton spends more time transitioning between sites. As both types of methyl groups present the same EISF, it does not appear likely that more frequent transitions lead to deviations from 3-fold rotation. On the other hand, both methyl groups execute librational motions approximately ±30 degrees from the jump site. This would have the effect of smearing out the apparent shape of the motion from a triangle [3-fold rotation] to a hexagon [6-fold rotation], as illustrated in Figure 8. The reasonable agreement between our simulation data and the predicted EISF for CH_3 rotation validates both the utility of the simulation and our method for isolating rotational motion.

In order to perform a quantitative analysis of CH_3 rotation, the portion of the decay curve attributed to this motion is fit with:

$$S(q,t) = A\left\{\text{EISF} + (1 - \text{EISF}) \exp\left[-\left(\frac{t}{\tau_{\text{KWW}}}\right)^{\beta}\right]\right\} \quad (6)$$

where A is the prefactor describing the first decay, τ_{KWW} the relaxation time, β the distribution of relaxation times, and the EISF is taken from the long time plateau of the $S(q,t)$ decay curve. All rotational times reported here are the τ_{KWW} resulting directly from fitting with eq 6. As discussed in ref 15, the stretched exponential function accounts for the existence of a distribution of rotational frequencies instead of a single rotational frequency, and provides more reasonable results than a single exponential when applied to QENS measurements.

Times for rotation are expected to be q independent with an Arrhenius temperature dependence. As seen in Figure 9a, the relaxation times fit with eq 6 for both α-methyl and ester methyl group rotations at 500 K verify the independence of spatial scale, with the ester rotation being much faster than the α rotation as is known experimentally. Figure 9b shows that β values for both methyl rotations are not sensitive to q.

The Arrhenius temperature dependence of rotation times is illustrated in Figure 10. We also include neutron[15] and NMR data[41] for comparison. As can be seen from the graph, both rotations are Arrhenius in temperature

$$\ln \tau = \ln \tau_0 + \frac{E_a}{RT} \quad (7)$$

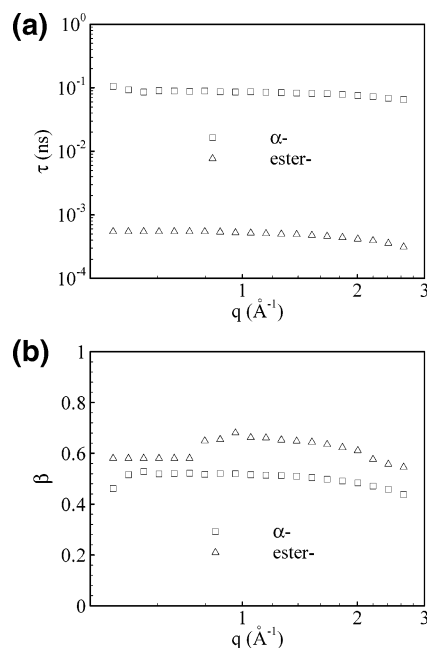where E_a is the activation energy. The activation energy calculated from eq 7 for α-methyl group rotation as shown in

Figure 9. q dependence of (a) rotation times and (b) β parameter for both α-methyl and ester CH_3 rotations at 500 K.

Figure 10a is 36.6 kJ/mol, close to the value of 34 kJ/mol derived by Higgins and Benoît[41] and the value of 32 kJ/mol reported by Allen et al.[42] As is clear from the figure, the α-methyl rotational times are very consistent with those from neutron scattering[41] and its rotational behavior at high temperature is obviously a continuation of that from NMR measurements[41] at low temperatures. For ester methyl group rotation as shown in Figure 10b, the activation energy is 8.9 kJ/mol, which is close to 10 kJ/mol reported from NMR experiments[18] although further from the 5.4 kJ/mol obtained from QENS measurements[15] and 5.9 kJ/mol obtained from inelastic neutron measurements[14] at low temperatures. MD and NS[15] relaxation times in Figure 10c for the ester CH_3 rotation fall on a smooth curve, and a change in activation energy seems hinted by the experimental data at around 160 K.

Plotted in Figure 10d are the stretching parameters for both ester and α-methyl group rotations as a function of temperature. In the case of the ester group, there is little difference with temperature, while for the α-methyl, a slight increase with increasing temperature is evident. The ester methyl rotation was analyzed using a stretched exponential in ref 15, and we note that the stretching parameter is observed to increase slightly and level off around 0.6 at temperatures above 200 K. This is consistent with our results.

Our results provide relaxation times of α-methyl and ester methyl group rotations at high temperatures. The main characteristics of methyl rotations are observed: q independent relaxation times, an EISF close to theoretical predictions, and Arrhenius temperature dependence of relaxation times. The range of our simulations is limited to temperatures well above T_g. Over the investigated temperature range, the activation energy for the ester methyl rotation is higher than that obtained from neutron scattering experiments.[15] Potential explanations apart from a change in activation energy as mentioned above are the different molecular weight or tacticity of the simulated sample. Rotation of methyl groups is very local and should not depend on molecular weight. Both rotation times and activation energies depend on tacticity. However, the barrier for rotation of isotactic PMMA is higher than that of syndiotactic PMMA[43] so the higher activation energy in our simulated systems [100% CDV
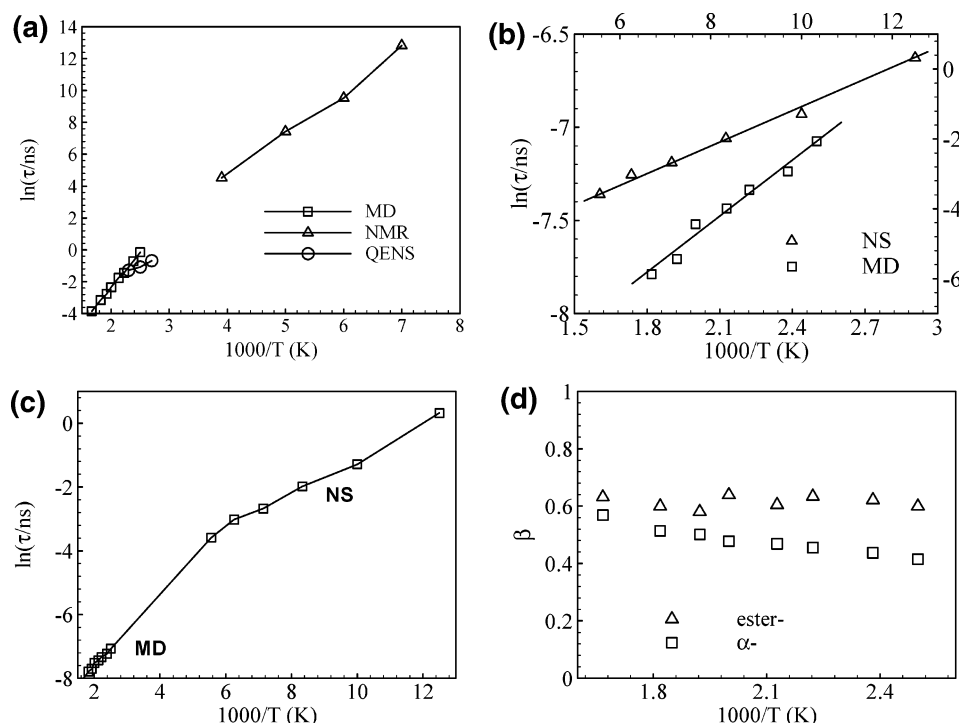
Figure 10. Temperature dependence of relaxation times and the β parameter for CH$_3$ group rotations at $q = 1.5$ Å^{-1}: (a) α-methyl rotation, and its comparison with NMR and QENS results;[41] (b) ester where the MD and neutron data[15] are plotted on separate scales; (c) ester, with neutron and MD data on a common scale; (d) β parameter for both methyl group rotations.
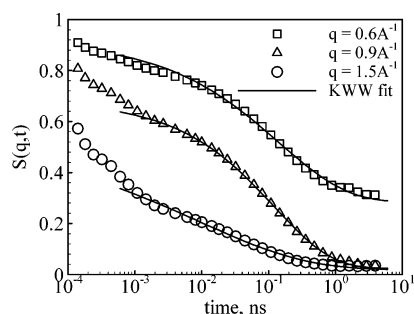

Figure 11. $S(q,t)$ for the rotation of ester hydrogen atoms around C–C bond connecting to the main chain at 600 K and at three q values. The KWW fits shown in this graph are only for the long time decay ($t > 1$ ps).

Figure 12. q dependence of the simulated EISF for rotation of the entire ester group rotation at 600 K, compared to the isotropic rotational diffusion model, where $r = 2.85$ Å^{-1}.

syndiotactic] would be expected to be lower than the experiments [predominantly syndiotactic].[15]

B. Entire Carboxyl Group Rotation. As discussed in the Introduction, the β-relaxation is prominent in the dielectric spectra of PMMA, and it has been associated with hindered rotation of the –COOCH$_3$ group around the C–C bond linking it to the main chain.[10] By isolating this specific motion and studying the resulting spectra, we tested this idea. This motion is isolated by considering the motion of the ester hydrogens relative to carbon C$_1$ [see Figure 1]. The $S(q,t)$ for ester side group rotation is thus calculated from the positions of the three hydrogen atoms relative to this carbon atom. This calculation, explicitly excludes rearrangement of the main chain, thereby separating the structural relaxation from carboxyl group rotation. Structural relaxation is addressed in section C. Figure 11 shows the rotational $S(q,t)$ for the entire ester group at 600 K and at three q values (0.6, 0.9, and 1.5 Å^{-1}). As with CH$_3$ group rotation, fast vibrations appear at short times. The rotation of the ester CH$_3$ group also contributes. A plateau in $S(q,t)$, i.e., the EISF, is again observed at longer times; however, in this case, its value is much smaller than that for CH$_3$ group rotation.
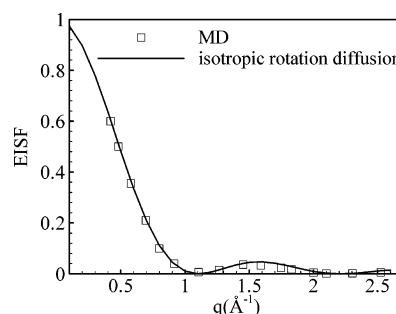
Because the rotating protons are separated from the point of rotation by three bonds, we expect the rotation to occur not through discrete jumps, but instead in a more continuous manner. In addition, the area of rotation should be larger. To test these ideas, we fit the EISF obtained from the plateau values of $S(q,t)$ to the prediction of the isotropic rotational diffusion model, in which continuous small angle rotations occur and the rotating molecule has no preferred spatial orientation.[39]

$$EISF = \left(\frac{\sin(qr)}{qr}\right)^2 \tag{8}$$

In the above equation, r represents the radius of the area of rotation. As shown in Figure 12, simulation data agree well with the isotropic rotational diffusion prediction with $r = 2.85$ Å. This suggests that ester methyl protons rotate around the C$_1$–C bond by randomly moving throughout a circle of radius 2.85 Å. Both the continuous nature of the motion and the size of the circle are a result of the two intervening bonds. Intramolecular packing in PMMA causes a broad second peak in $S(q)$ corresponding to length scales of approximately 3 to 4.5 Å. This likely reflects the length scales involved in packing of adjacent
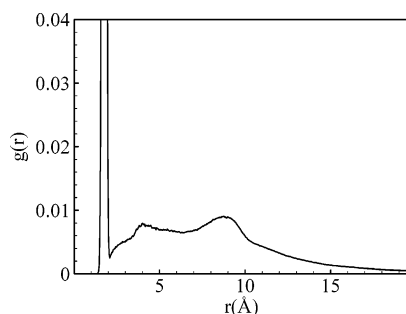
CDV

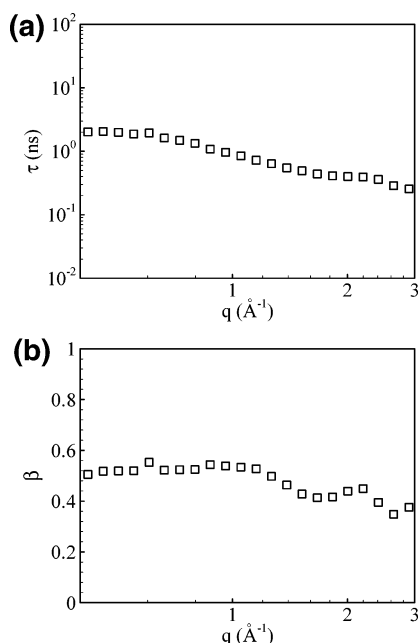**Figure 13.** Intramolecular pair distribution function between ester protons at 500 K.

Figure 14. *q* dependence of relaxation times and stretching exponents for rotation of the entire ester side group at 500 K.

Figure 15. Comparison of the temperature dependence of entire ester side group rotation behavior to DS β-relaxation:[44] (a) τ vs 1000/T; (b) β vs T.

ester groups. Thus, it is reasonable that the ester group is confined to a circle of radius slightly less than 3 Å. To test this idea, we show the pair distribution function [Figure 13] between ester protons on the same chain. The peak at ∼4 Å is consistent with the spatial extent of rotation indicated by EISF.

Since rotation is slower for the entire ester group, the plateau in $S(q,t)$ can only be clearly ascertained within 6 ns for 600 K, and thus other temperatures are not shown. We expect that the EISF is independent of temperature, and have used the value from 600 K, along with eq 6 to fit ester group rotation at all temperatures. In Figure 14 we show the spatial dependence of the relaxation times and stretching parameters obtained in the fits. The relaxation times are only weakly *q* dependent, as expected for rotation. The stretching parameters cluster around 0.43, consistent with dielectric measurements of the β-relaxation for which $\beta = 0.45$ at 475 K.[44] Figure 15 shows the temperature dependence of relaxation times and β for the ester group rotation. In Figure 15b, we plot the stretching parameter obtained from fits of ester side group motion with that obtained from dielectric spectroscopy [DS] data for the β-relaxation[44] at two *q* values (0.6 and 1.5 Å^{-1}). Our results show the same trend with temperature over the range where DS data is available. The activation energy calculated using eq 7 does not depend on *q* and has a value of 77.4 kJ/mol, which is consistent with the 79.42 kJ/mol for the β process at temperatures below T_g from dielectric spectroscopy.[44] Figure 15a compares the relaxation
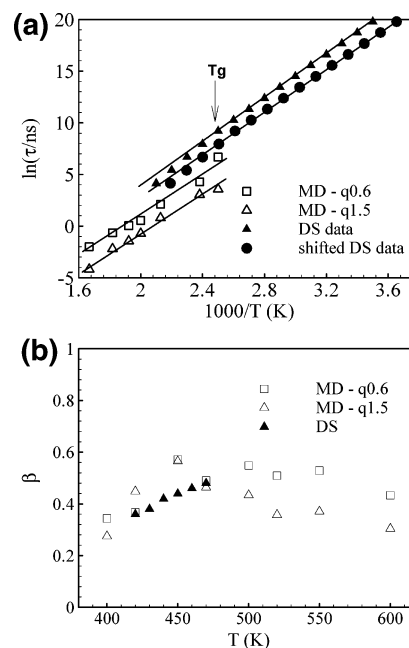
times obtained from the above analysis of ester group rotation and dielectric spectroscopy measurements of the β-relaxation. It is apparent that the slopes are co-incident but the values of relaxation times are not in agreement. Because the T_g of PMMA is molecular weight and tacticity dependent, the T_gs of the simulated and measured (M_w 550 000, T_g 404 K) samples differ by approximately 17 K. To test if this might have an influence, we have shifted the DS data to account for this difference. While one would expect that the β-relaxation is a local process, independent of effects from slowing of segmental motion at T_g, it does appear that the actual times are more consistent with experimental data if the latter are shifted. This is consistent with the finding that ester group rotation is accompanied by main chain rearrangement.[10] It is interesting that even for temperatures well below T_g, where main chain motion should be arrested, the dielectric data must be shifted to be consistent with the high-temperature simulation data where main chain motion is omitted from the calculation. In the temperature range of our simulations, the β-relaxation is merged with the α-relaxation in dielectric measurements. The merged process has an activation energy of 110 kJ/mol. For the simulation results, in this temperature range, the rotation of the ester side group appears to be a high temperature isolation of the local motion responsible for the β-relaxation, and thus its activation energy is consistent with that of the β process measured via dielectric spectroscopy at low temperatures, where its motion is not coupled with main chain reorientation. This confirms that its origin is rotation of the ester group, as has been suggested previously. In ref 10, the β-relaxation is described as consisting of 180° side group flips, accompanied by rotational readjustments of the main chain. These adjustments are not included in the scattering function calculated for the rotation of the ester group. However, if, as is argued in ref 10, the ester group rotation only occurs with corresponding main chain motion, then this is included implicitly in the rates because the rotation would not occur in absence of torsional rearrangement. At least with respect to the rotation of the ester protons, 180° flips [2-site rotation] as suggested in ref 10, are not consistent with our data. As with rotation of the methyl groups, we present in Figure 16 the torsional angle
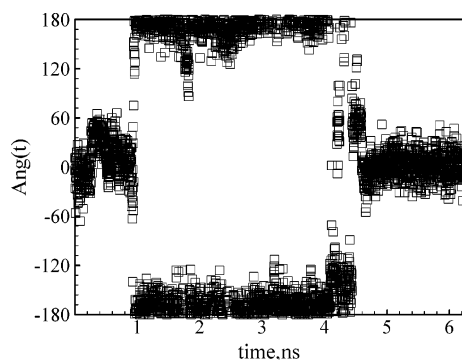
Figure 16. Torsional angle involving rotation of the ester oxygen around the C$-$C$_1$ bond (C$_3-$C$_1-$C$-$O) as a function of time with the time interval of 2 ps at 500 K.
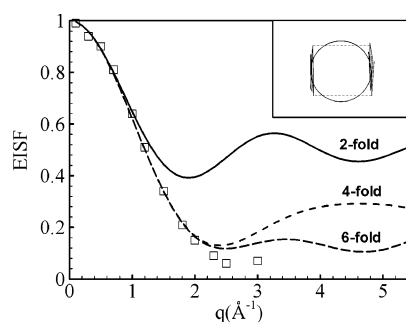

Figure 17. EISF from ester oxygen rotation compared to theoretical predictions from 2-fold, 4-fold, and 6-fold models, where r_{O-O} is 2.1 Å. Inset picture represents an approximated 4-fold jump.
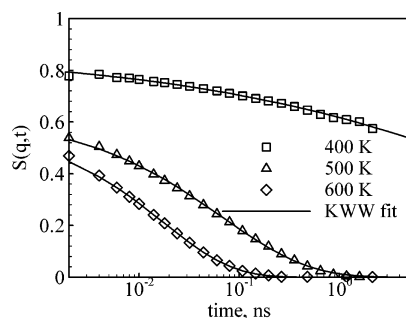

Figure 18. Main chain relaxation processes at different temperatures and $q = 1.5$ Å^{-1}.

involving rotation of the ester oxygen around the C$_1-$C bond [O$-$C$-$C$_1-$C$_3$]. Although the sampling time is small compared to the residence time in each site, two sites are visited, consistent with a 180° flip. Moreover, librations within these sites lead to torsional angle variations of ±60°. As with methyl group rotation, this variation smears out the apparent site such that the shape visited by the ester oxygen more resembles a square [4-fold rotation] as shown in Figure 17.

C. Main Chain Dynamics. The α-relaxation is often associated with the chain backbone. To test this for PMMA, we investigate the main chain dynamics by including only hydrogen atoms on the main chain when computing $S(q,t)$. The resulting decay curves are shown in Figure 18. As expected, main chain motion is highly temperature dependent. For the highest temperatures, $S(q,t)$ decays to zero at long times for all q values, indicating there is no EISF as expected. We thus fit the main chain decay with,

$$S(q,t) = A \exp\left[-\left(\frac{t}{\tau_{KWW}}\right)^{\beta}\right] \quad (9)$$

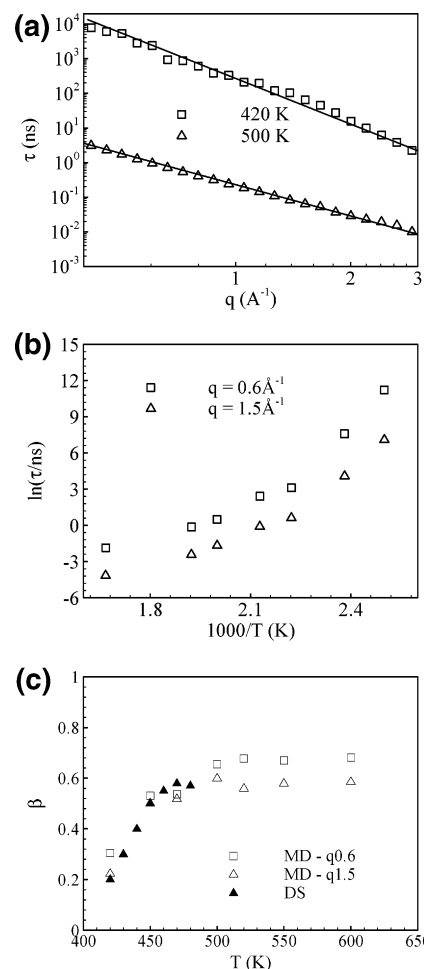**Figure 19.** Main chain motion dynamics: (a) q dependence of relaxation times; (b) T dependence of relaxation times; (c) T dependence of β parameter and its comparison to DS data.

As with rotational times, all times reported for main chain relaxation are the τ_{KWW} times resulting directly from fits to eq 9. Good agreement is found between our simulation data and the DS data, as shown in Figure 19. They all suggest that the α-relaxation is more strongly temperature dependent than the β-relaxation, and that the α-relaxation is less stretched at high temperatures. The q dependence of relaxation times as shown in Figure 19a, as well as all the other temperatures, follows $\tau \propto q^{-2/\beta}$, which is often observed for the α-relaxation in polymers.[45] Our prior neutron measurements[11] showed that $\tau \propto q^{-2/\beta}$ is expected at temperatures within 40 K of T_g. The temperature dependence of relaxation times, as shown in Figure 19b for two q values, is obviously non-Arrhenius. These results suggest that the motion of the chain backbone is the primary contribution to the α-relaxation in PMMA. The time scale of this motion is co-incident with that of ester group rotation in the higher end of the temperature range, as can be seen in Figure 20. This is expected from the merging of α- and β-relaxations in DS. At higher spatial scales, rotation of the α-methyl also appears on the same time scales. We will return to this figure below. The stretching parameter obtained from fits of main chain motion is compared to that obtained from DS for the α-relaxation in Figure 19c. The comparison indicates again and emphasizes the correlation between main chain motion and the α-relaxation.

D. Comparison with Dielectric and Backscattering Measurements. In addition to considering the four motions described above on an individual basis, we have also calculated the
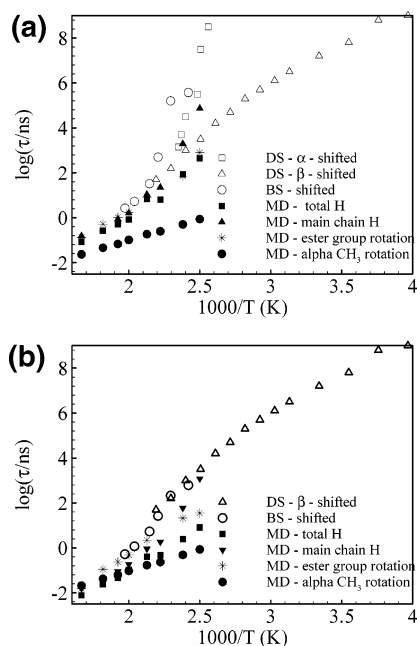
CDV

Figure 20. Comparison of simulation data to dielectric[44] and neutron scattering[11] results at: (a) $q = 0.6$ Å^{-1}; (b) $q = 1.5$ Å^{-1}.

Figure 21. Summary of temperature dependence of relaxation times for different relaxations at: (a) $q = 0.6$ Å^{-1}; (b) $q = 1.5$ Å^{-1}.

scattering function $S(q,t)$ including all hydrogens. This decay is fit with eq 9, with both the simulation data and the fit lines shown in Figure 4. This result would compare directly to the neutron measurement in ref 11. Three of the individual motions we address here have comparable time scales and should contribute to this overall decay. The overall relaxation is thus compared with ester group rotation, the main chain motion, and α-CH$_3$ group rotation in Figure 20. Experimental data, from both QENS and DS, are also shown. The experimental data, both QENS and DS, have been shifted to account for differences in T_g. Figure 20a illustrates a spatial value, $q = 0.6$ Å^{-1}, larger than the interchain spacing. Here the rotations do not contribute as much (the EISF is 0.88 for methyl group rotation and 0.36 for ester group rotation), and thus the α-methyl rotation time does not influence the decay of all protons to a large extent. This can be seen by comparing the times for all proton motion, main chain motion, and α-methyl group rotation in Figure 20a. Although the α-methyl rotation times are quite different, they do not contribute much to the decay calculated with all protons. This is the reason that this spatial scale shows α-relaxation character. This is also the spatial scale which most closely agrees with relaxation times from DS, and accordingly these times are also given. In Figure 20b, we illustrate a smaller spatial scale, $q = 1.5$ Å^{-1}. Although DS data are more consistent with QENS at $q = 0.6$ Å^{-1}, we also show this data here to facilitate comparison with the β-relaxation. Here the EISF for methyl rotation is 0.4 and that for ester rotation is 0.05. As a result, both β-relaxation [rotation of the ester side group] and rotation of the α-CH$_3$ group contribute more than at $q = 0.6$ Å^{-1}. Since both are Arrhenius, the overall decay appears more skewed toward the β-relaxation. This is the reason the experimental QENS data appears more consistent with the β-relaxation at large q.

VI. Summary and Conclusion

Although a variety of experiments are available to explore the dynamics of methyl group rotation, the β-relaxation and the α-relaxation in PMMA, it is difficult to retrieve specific local motions using these techniques because the response in a particular experiment includes all types of motion grouped
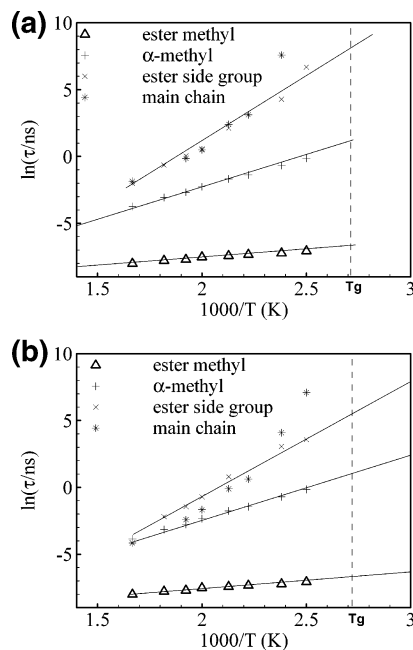
together. This is particularly true at temperatures above T_g. Here we have adopted molecular dynamics simulations to isolate several motions in PMMA, which is both well studied and has several important applications due to its high transparency in visible light. We evaluate the performance of our EA model for both static and dynamic observables using neutron scattering data. The performance of this model is comparable and in agreement with neutron diffraction for static properties. The dynamics represented via QENS experiments are also in reasonable agreement. We use the model to study four different molecular motions in PMMA: main chain motion, rotation of the ester side group, and rotation of both methyl groups. Our main conclusions are summarized in the form of the Arrhenius plots for the relaxation times of all four motions in Figure 21. An Arrhenius temperature dependence is evident for all three rotations: the α-methyl, the ester methyl and the entire ester side group. The activation energies follow ester side > α-methyl > ester methyl, consistent with available data. Further, α-methyl and ester methyl activation energies approach values reported in literature, and, as shown in Figure 10, both rotational times agree well with experimental measurements. The activation energy for the entire ester side group rotation is consistent with the value reported for the β-relaxation measured from dielectric experiments. We confirm that the β-relaxation originates from rotation of the ester side group, as first suggested from NMR experiments. This rotation contributes with the same activation energy above T_g. Finally motion of the main chain does not show Arrhenius temperature dependence but rather diverges as T_g is approached. The spatial dependence of main chain relaxation times follow $\tau \propto q^{-2/\beta}$, indicative of translational motion. Both of these observations support the idea that the α-relaxation is associated with the motion of the main chain in PMMA.

CDV

References and Notes

(1) Bieze, T. W. N.; Vandermaarel, J. R. C.; Eisenbach, C. D.; Leyte, J. C. *Macromolecules* **1994**, *27*, 1355.
(2) Gómez, D.; Alegría, A.; Arbe, A.; Colmenero, J. *Macromolecules* **2001**, *34*, 503.
(3) Merenga, A. S.; Papadakis, C. M.; Kremer, F.; Liu, J.; Yee, A. F. *Colloid Polym. Sci.* **2001**, *279*, 1064.
(4) Arbe, A.; Colmenero, J.; Monkenbusch, M.; Richter, D. *Phys. Rev. E.* **1996**, *54*, 3853.
(5) Zhu, W.; Gisser, D. J.; Ediger, M. D. *J. Polym. Sci., Polym. Phys.* **1994**, *32*, 2251.
(6) Arbe, A.; Monkenbusch, M.; Stellbrink, J.; Richter, D.; Farago, B.; Almdal, K.; Faust, R. *Macromolecule*s **2001**, *34*, 1281.
(7) Karatasos, K.; Saija, F.; Ryckaert, J.-P. *Physica. B* **2001**, *301*, 119.
(8) Ritchter, D.; Arbe, A.; Colmenero, J.; Monkenbusch, M.; Farago, B.; Faust, R. *Macromolecules* **1998**, *31*, 1133.
(9) Karatasos, K.; Ryckaert, J.-P.; Ricciardi, R.; Lauprêtre, F. *Macromolecules* **2002**, *35*, 1451.
(10) Schmidt-Rohr, K.; Kulik, A. S.; Beckham, H. W.; Ohlemacher, A.; Pawelzik, U.; Boeffel, C.; Spiess, H. W. *Macromolecules* **1994**, *27*, 4733.
(11) García Sakai, V.; Chen, C. X.; Maranas, J. K.; Chowdhuri, Z. *Macromolecules* **2004**, *37*, 9975.
(12) Prager, M.; Heidemann, A. *Chem. Rev.* **1997**, *97*, 2933.
(13) Moreno, A. J.; Alegría, A.; Colmenero, J.; Prager, M.; Grimm, H.; Frick, B. *J. Chem. Phys.* **2001**, *115*, 8958.
(14) Moreno, A. J.; Alegría, A.; Colmenero, J.; Frick, B. *Macromolecules* **2001**, *34*, 4886.
(15) Arrighi, V.; Higgins, J. S.; Burgess, A.; Howells, W. S. *Macromolecules* **1995**, *28*, 2745.
(16) Arrighi, V.; Higgins, J. S. *Physica. B* **1996**, *226*, 1.
(17) Allen, G.; Higgins, J. S. *Rep. Prog. Phys.* **1973**, *36*, 1073.
(18) Heijboer, J.; Baas, J. M. A.; van de Graaf, B.; Hoefnagel, M. A. *Polymer* **1987**, *28*, 509.
(19) Soldera, A. *Macromol. Symp.* **1998**, *133*, 21.
(20) Apel, U. M.; Hentschke, R.; Helfrich, J. *Macromolecules* **1995**, *28*, 1778.
(21) Soldera, A.; Metatla, N. *Composites, Part A: Appl. Sci.* **2005**, *36*, 521.
(22) Berendsen, H. J. C.; Postma, J. P. M.; Van Gunsteren, W. F.; Di Nola, A.; Heak, J. R. *J. Chem. Phys.* **1984**, *81*, 3684.
(23) Wunderlich, W. In *Polymer Handbook*, 3rd ed.; Brandrup, J., Immergut, E. H., Eds.; John Wiley & Sons: New York, 1989; Sec. 5, p 77.
(24) Price, M. L. P.; Ostrovsky, D.; Jorgensen, W. L. *J. Comput. Chem.* **2001**, *22*, 1340.
(25) Kahn, K.; Bruice, T. C. *J. Comput. Chem.* **2002**, *23*, 977.
(26) Ewald, P. *Ann. Phys.* **1921**, *64*, 253.
(27) Abdulnour, Y.; Toukmaji, J. A.; Board, J. A., Jr. *Comput. Phys. Commun.* **1996**, *95*, 73.
(28) Humphreys, D. D.; Friesner, R. A.; Berne, B. J. *J. Phys. Chem.* **1994**, *98*, 6885.
(29) Tuckerman, M.; Berne, B. J.; Martyna, G. J. *J. Chem. Phys.* **1992**, *97*, 1990.
(30) Farago, B.; Chen, C. X.; Maranas, J. K.; Kamath, S.; Colby, R. H.; Pasquale, A. J.; Long, T. E. *Phys. Rev. E* **2005**, *72*, 031809.
(31) Meyer, A.; Dimeo, R. D.; Gehring, P. M.; Neumann, D. A. *Rev. Sci. Instrum.* **2003**, *74*, 2762.
(32) Copley, R. D.; Cook, J. C. *Chem. Phys.* **2003**, *292*, 477.
(33) The IDL-based program can be found at http://www.ncnr.nist.gov/dave.
(34) García Sakai, V.; Maranas, J. K.; Chowdhuri, Z.; Peral, I.; Copley, J. R. D. *J. Polym. Sci., Part B: Polym. Phys.* **2005**, *43*, 2914.
(35) Borodin, O.; Douglas, R. J.; Smith, G. D.; Trouw, F.; Petrucci, S. *J. Phys. Chem. B.* **2003**, *107*, 6813.
(36) Genix, A. -C.; Arbe, A.; Alvarez, F.; Comenero, J.; Willner, L.; Richter, D. *Phys. Rev. E.* **2005**, *72*, 031808.
(37) Pérez Aparicio, R.; Arbe, A.; Colmenero, J.; Frick, B.; Willer, L.; Ritchter, D.; Fetters, L. J. *Macroleculess* **2006**, *39*, 1060.
(38) Saelee, C.; Nicholson, T. M.; Davies, G. R. *Macromolecules* **2000**, *33*, 2258.
(39) Bée, M. *Quasielastic Neutron Scattering*; Adam Hilger: Bristol, U.K., 1988.
(40) Zorn, R.; Frick, B.; Fetters, L. J. *J. Chem. Phys.* **2002**, *116*, 845.
(41) Higgins, J. S.; Benoît, H. C. *Polymers and Neutron Scattering;* Clarendon Press: Oxford, U.K., 1994.
(42) Allen, G.; Wright, C. J.; Higgins, J. S. *Polymer* **1974**, *15*, 319.
(43) Cereghetti, P. M.; Kind, R.; Higgins, J. S. *J. Chem. Phys.* **2004**, *121*, 8068.
(44) Bergman, R.; Alvarez, F.; Alegría, A.; Colmenero, J. *J. Chem. Phys.* **1998**, *109*, 7546.
(45) Richter, D. *Macromol. Symp.* **1997**, *121*, 147.